PHYSICAL REVIEW B **96**, 020409(R) (2017)

Three-dimensional dispersion of spin waves measured in NiO by resonant inelastic x-ray scattering

D. Betto,[1,*] Y. Y. Peng,[2] S. B. Porter,[3] G. Berti,[2,†] A. Calloni,[2] G. Ghiringhelli,[2,4] and N. B. Brookes[1]

[1]*European Synchrotron Radiation Facility, 71 Avenue des Martyrs, Grenoble, France*

[2]*Dipartimento di Fisica, Politecnico di Milano, Piazza Leonardo da Vinci 32, I-20133 Milano, Italy*

[3]*CRANN and AMBER, Trinity College, Dublin 2, Ireland*

[4]*CNR-SPIN and CNISM, Politecnico di Milano, Piazza Leonardo da Vinci 32, I-20133 Milano, Italy*

(Received 12 June 2017; published 20 July 2017)

We used resonant inelastic x-ray scattering (RIXS) at the Ni L_3 edge to measure the dispersion of spin waves in NiO thin films along the [101], [001], and [111] directions. Samples with tensile and compressive in-plane strain show identical dispersion within the experimental uncertainty. The fitting of the data with a linear spin wave model applied to a three-dimensional Heisenberg antiferromagnetic lattice provides a leading superexchange parameter $J' = 18$ meV. The magnon energy at the Brillouin zone boundary and the value of J' are 5% smaller than those determined by inelastic neutron scattering on bulk single crystals. This discrepancy is likely induced by the strain or other structural differences between bulk and epitaxially grown samples. These results demonstrate the capabilities of high-resolution RIXS in the study of the magnetic structure of thin films and heterostructures for which neutron scattering is not sensitive enough.

DOI: 10.1103/PhysRevB.96.020409

I. INTRODUCTION

The technique of choice for the measurement of spin wave dispersions in magnetic materials is usually inelastic neutron scattering (INS). While this method is routinely applied, it has several limitations, such as the loss of energy resolution at higher-energy transfers and the need for background subtraction. The most important drawback concerns the size of the sample: Given the very small scattering cross section of neutrons, INS requires large bulk samples in order to obtain a reasonable signal intensity, excluding a significant number of technologically relevant materials which are employed in thin-film form. Owing to the improvement in energy resolution, in recent years, resonant inelastic x-ray scattering (RIXS) at the L_3 edge of transition metals has been successfully used to investigate magnetic excitations, especially in high-temperature superconducting cuprates [1–4].

NiO is a prototypical example of an insulating antiferromagnet. It crystallizes in the simple cubic rocksalt structure, with a lattice constant $a_0 = 4.177$ Å. The Ni^{2+} ions have a nominal $3d^8$ electronic configuration, with the cubic crystal field and electron-electron interactions stabilizing a high-spin $^3A_{2g}$ ground state, with spin $S = 1$. Ni sites form an fcc sublattice where the magnetic configuration is determined by nearest- and next-nearest-neighbor interactions, J and J' (Fig. 1). The latter is an antiferromagnetic superexchange interaction mediated by the 180° Ni-O-Ni bonds and it is the leading parameter, while J has been reported to be much smaller and, given the 90° Ni-O-Ni bonds, ferromagnetic. The magnetic structure of NiO has been thoroughly investigated in the past [5], mainly by neutron diffraction and inelastic scattering. The type-II antiferromagnetic configuration consists of ferromagnetic sheets of spins in the (111) planes, while the spins themselves lie along the $\langle 11\bar{2}\rangle$ directions, i.e., they lie in the ferromagnetic planes [Fig. 1(a)]. Untreated samples can potentially possess up to 24 different kinds of domains [6–10]: four T domains corresponding to the equivalent $\langle 111\rangle$ directions of the ordering vector, three in each plane of the possible $\langle 11\bar{2}\rangle$ orientations of the spins, and for each of these there is an equivalent inversion of the spin direction. It is very difficult to obtain a single domain in a macroscopic sample, which complicates the experiments. In thin films, the equivalence of the crystallographic directions can be partially removed by exploiting the exchange interaction arising at the interface with a ferromagnetic substrate [11] or even the strain involved in the epitaxial growth of the NiO films [12], therefore inducing preferential spin orientations. These samples, however, are not measurable by INS. NiO is very often used as a benchmark material to put to the test *ab initio* theories for the exchange coupling and spin wave spectrum of strongly correlated oxides [13–19]. Nonetheless, the experimental data regarding spin wave dispersions that can be found in the literature are quite scarce [10].

Following the theoretical predictions of Ref. [20], spin excitations have been previously measured in bulk single crystal NiO by Ghiringhelli *et al.* [21]: The authors could not see dispersing excitations but found two nondispersing peaks which they attributed to localized single and double spin-flip events.

Here, we utilized the new capabilities of the beamline ID32 at the ESRF to measure high-resolution RIXS spectra at the L_3 edge of Ni in NiO thin films. Making a compromise between the highest possible energy resolution and counting time, the experimental setup allows for a resolution ∼40 meV at the Ni L_3 edge. Another key feature is the three-circle high-precision sample manipulator combined with the continuous variation of the θ-2θ scattering angles without breaking the vacuum. Thus we have been able to precisely map the spin wave dispersion in different reciprocal lattice directions in thin-film samples.

*davide.betto@esrf.fr

†Present address: Department of Chemical Physics, Fritz-Haber-Institut der Max-Planck-Gesellschaft, Faradayweg 4-6, 14195 Berlin, Germany.

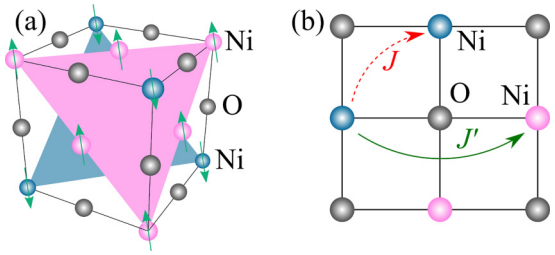

FIG. 1. (a) NiO crystal and magnetic structures. (b) Schematic representation of the exchange interactions between Ni atoms in a (001) plane of NiO. J is the nearest-neighbor interaction, and J' is the next-nearest-neighbor interaction.

II. EXPERIMENTAL DETAILS

Spin wave dispersions have been measured in 31- and 37-nm-thick films of NiO grown on (001)- and (011)-oriented MgO, respectively, by pulsed laser deposition (PLD) [22], and a ∼50-nm-thick film grown on a (001)-oriented Au crystal by molecular beam epitaxy (MBE) [23]. The NiO layers grow in a cube-on-cube fashion on these substrates, as confirmed by x-ray diffraction (XRD) and low-energy electron diffraction (LEED). The lattice parameter of Au is 4.07 Å, the one of MgO is 4.21 Å, while we have $a_0 = 4.177$ Å for bulk NiO. Thus, from the bulk lattice parameters we estimate that NiO films are under 0.96% tensile strain on MgO and 2.3% compressive strain on Au.

The RIXS spectra have been measured at the ID32 beamline [24] at the European Synchrotron (ESRF), as mentioned previously. The x-ray energy was tuned to the peak of the Ni L_3 edge, at about 853 eV. This choice of incoming energy maximizes the scattered intensity of the single magnon [21]. Each spectrum is the result of accumulation for 30–60 min. The x-ray absorption spectra (XAS) have been measured by total electron yield. The pressure in the sample chamber was lower than 1×10^{-9} mbar and the measurement temperature was ∼20 K. The total resolution in energy was about 40 meV, while the resolution in the reciprocal space wave vector was 4×10^{-3} Å^{-1} or better. The spot size of the beam was about 4×30 μm^2. The experimental geometry is shown in Fig. 2. The scattering angle was varied from 54° to 145° and the x-ray beam was linearly polarized within (H) or normal to (V) the horizontal scattering plane. The θ angle was adjusted to be half the scattering angle in each point. Strong elastic reflection from the surface was avoided by tilting the sample with the χ rotation (see Fig. 2), so that the normal to the surface was never lying in the scattering plane. The samples grown on MgO substrates with (001) orientation have been tilted by an angle $\chi = 45°$ around the [010] axis to measure the dispersions along the [101], while the sample grown on MgO with (011) orientation has been tilted by 45° around the [100] axis for the [001] dispersion and by ∼34° around the [0$\bar{1}$1] axis for the [111] dispersion. For the sample grown in the Au (001) substrate we followed a straight trajectory close (10°) to the [111] direction. This slight deviation has been taken into account in the spin wave dispersion calculations discussed in Sec. III and in Fig. 5.

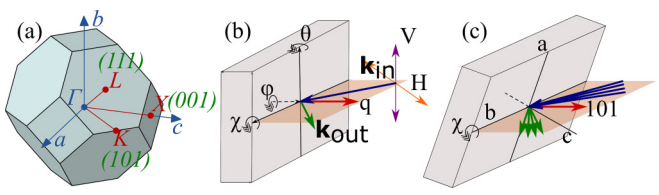

FIG. 2. (a) First Brillouin zone and reciprocal space directions that will be investigated. (b) Generic RIXS measurement geometry, showing the rotation angles θ, φ, and χ. (c) Measurement geometry for the [101] dispersion, after rotation of the sample around χ.

RIXS is a *photon-in photon-out* process [25] which, in our case, can be described as a combination of the XAS process ($2p^6 3d^8 \rightarrow 2p^5 3d^9$) and a subsequent radiative decay (typically after a few fs) to a $2p^6 3d^{8*}$ state, which represents the ground state or an excited state of the initial configuration. Tuning the incoming energy to a transition edge of an atom increases by orders of magnitude the inelastic scattering cross section, making it an element-specific resonant process. The technique allows for the simultaneous measurement of the change in energy ($\Delta E = E_{\text{out}} - E_{\text{in}}$), polarization ($\Delta\epsilon = \epsilon_{\text{out}} - \epsilon_{\text{in}}$), and wave vector ($\vec{Q} = \vec{k}_{\text{out}} - \vec{k}_{\text{in}}$) of the photons. Since RIXS is a second-order process, it is not limited to dipole selection rules, so that intraband transitions (dd excitations) are allowed and usually dominate the spectra [26]. At the L edges, the strong spin-orbit interaction of the core level allows for the coupling between the angular momentum of the photons and the spin of the electrons, making it possible to excite spin-flip events and generate spin waves.

III. RESULTS AND DISCUSSION

The series of RIXS spectra for the NiO/MgO thin film is presented in Figs. 3(a) and 3(b) as a function of Q along the [111] direction. The dd excitations are clearly visible and in agreement with previous measurements [26] and theoretical studies [20]. The single magnon and double magnon peaks can also be clearly distinguished close to the elastic peak, which increases strongly in intensity towards lower Q values, i.e., in forward scattering geometry.

Both XAS and RIXS spectra can be well described using a multiplet ligand field theory by considering a Ni^{2+} ion

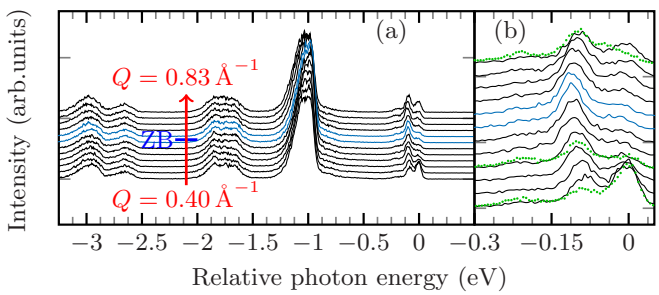

FIG. 3. (a) RIXS spectra of NiO/MgO with H polarization as a function of the Q vector along the [111] direction. (b) Close view of the low-energy part of the spectra. The spectra in blue correspond to Q vectors at the zone boundary (ZB). The spectra in green circles are from the NiO/Au sample and are superimposed on the respective NiO/MgO spectra.

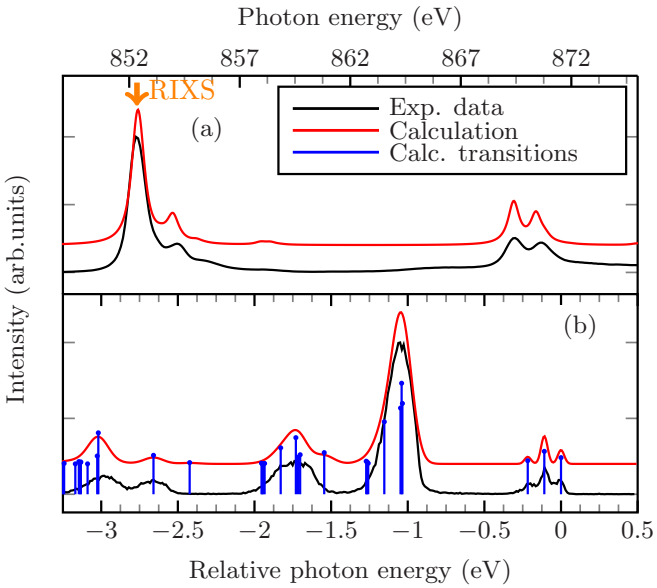

FIG. 4. Experimental and simulated absorption spectra (a) and RIXS at $Q = 0.83$ Å^{-1} along the [101] direction for NiO/MgO (b). The latter has been obtained by convolution with Gaussians to reproduce the experimental peak widths. The arrow in (a) indicates the chosen incident energy for the RIXS spectra.

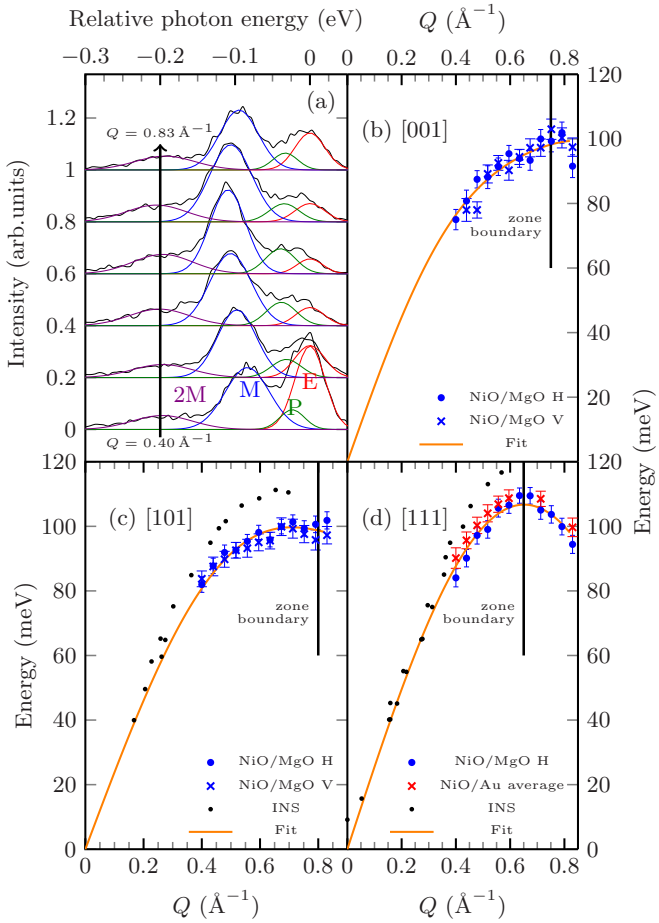

FIG. 5. (a) Low-energy features of the spectra in Fig. 3(a) with the decomposition into four Gaussians corresponding to elastic peak, phonons, magnon, and double magnon. They are labeled E, P, M, and 2M, respectively, on the lowest spectrum. (b) Spin wave dispersion along the [001] direction. (c) Spin wave dispersion along the [101] direction. (d) Spin wave dispersion along the [111] direction. The fits result from linear spin wave theory, as explained in the text. The INS data are taken from Ref. [10].

surrounded by six oxygen ions in an octahedral environment [27], as shown in Figs. 4(a) and 4(b). The uniaxial strain provided by the substrates has a negligible effect on the spectra. The nominal electronic configuration is $3d^8$ with an effective occupation number of ∼8.2 due to charge transfer from the ligands [28]. The calculation of Fig. 4 is an average of the spectra obtained from all equivalent in-plane spin orientations ($\langle \pm\bar{2} \pm 1 \pm 1\rangle$ and $\langle \pm 1 \pm \bar{2} \pm 1\rangle$). Linear dichroism spectra of the two samples showed that the NiO/MgO samples have preferential in-plane spin orientation, while the NiO/Au samples are in a more isotropic average spin arrangement [29,30]. Since the $^3A_{2g}$ ground state does not split in a cubic or tetrahedral crystal field, this linear dichroism is derived purely from the magnetic state and not from charge distribution effects.

The spectra for the NiO/Au sample are very similar, as can be seen in Fig. 3(b). The main difference is in the intensity of the elastic line, which is due to the quality of the surface and of the sample.

As shown in Fig. 5(a), the low-energy loss parts of the RIXS spectra have been decomposed into four principal Gaussian components. They correspond to, in order of increasing energy loss, the elastic line, the phonon peak(s), the single magnon peak ($\Delta S = 1$), and the double magnon peak ($\Delta S = 2$). The position of the peaks along the [101], [001], and [111] directions is shown in Fig. 6 for H polarization. According to Ref. [31], the optical phonons should give contributions at ∼54 and 69 meV, while, according to Ref. [32], the main phonon peak should be at 58 meV with quite small dispersion. We are only able to resolve a nondispersive mode at ∼40 meV. This peak has a full width at half maximum (FWHM) of approximatively 41 meV, due to the instrumental resolution. In contrast, the double magnon peak is very broad, with a FWHM of ∼150 meV. The center of this peak is found at around 190 meV, in good agreement with previous reports [31,33]. The width of the single magnon peak is not limited by the instrumental resolution and is found to be around 50–60 meV. Unlike the single magnon, we cannot distinguish a clear dispersion in the double magnon excitation. The conservation of total momentum requires that the sum of the momenta of two magnons is equal to the transferred momentum Q. Therefore, multiple combinations are possible and a broad bandlike feature is observed, without any dispersion. This is also in agreement with previous theoretical studies [4].

The dispersion of the single magnon peak is clearly observed and shown in Figs. 5(b)–5(d) for the [101], [001], and [111] directions, respectively. No significant difference is observed between the horizontal and vertical polarizations. However, as already observed with INS [10], the difference between different magnetic domain orientations cannot be resolved in this wave-vector range.

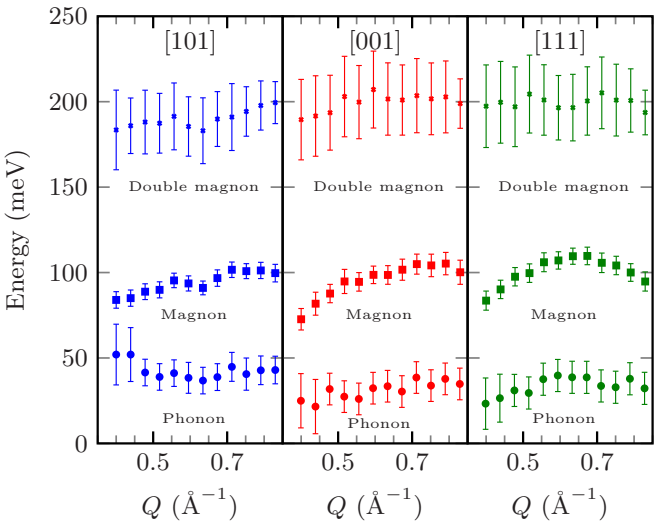

FIG. 6. Dispersions of the phonon, magnon, and double magnon peaks in NiO/MgO measured with H polarization along the [101], [001], and [111] directions. Both phonons and double magnons do not show any evident dispersion, the latter in agreement with Ref. [4].

The dispersion curves along the three directions can be well described by linear spin wave theory for a type-II fcc antiferromagnetic Heisenberg lattice with spin $S = 1$, using the equation [10]

$$\begin{aligned} E^2(q) &= A^2 - B^2, \\ A &= 6J' + 2JC_1, \\ C_1 &= \cos\tfrac{1}{2}a_0(q_x - q_y) + \cos\tfrac{1}{2}a_0(q_y - q_z) \\ &\quad + \cos\tfrac{1}{2}a_0(q_z - q_x), \\ B &= 2J'C_2 + 2JC_3, \\ C_2 &= \cos a_0 q_x + \cos a_0 q_y + \cos a_0 q_z, \\ C_3 &= \cos\tfrac{1}{2}a_0(q_x + q_y) + \cos\tfrac{1}{2}a_0(q_y + q_z) \\ &\quad + \cos\tfrac{1}{2}a_0(q_z + q_x). \end{aligned} \tag{1}$$

As previously reported [10,34], the leading exchange interaction is the one between next-nearest neighbors J'. A least-squares fitting of the dispersions gives a value of ∼18.1(4) meV, slightly smaller than the value of 19 meV found with INS [10]. The films grown on the two different substrates provide very consistent values of J', significantly different from those obtained on single crystals with neutrons. The reasons for this difference are more likely in the properties of the samples (thin films, strain that induces a lattice distortion or defects) than in the technique. In fact, this is the opposite of what was previously reported for the two-dimensional (2D) cuprate $Sr_2CuO_2Cl_2$ [35], where the comparison between RIXS and INS data shows that the former finds a higher magnon energy at the zone boundary in the [10L] direction. This was interpreted as a sign of the presence of other high-energy contributions in the RIXS spectra, which cannot be the case here. The extrapolated nearest-neighbor exchange interaction J has been found to be much smaller (of the order of 1 meV) and ferromagnetic, in agreement with previous literature.

IV. CONCLUSIONS

The dispersion curves shown in Fig. 5 are in very good agreement with previous publications [14,16]: In particular, the slightly different energies at the Brillouin zone boundary for the three directions and the presence of a maximum before the zone boundary along the [101] direction are clearly visible. This result shows that RIXS is complementary to INS in the investigation of magnetic excitations since it enables the measurement of these phenomena in thin films and allows for a clearer identification of the magnetic peaks without the need for background subtraction and other procedures, even at relatively high-energy transfers. In addition, it is an element-specific technique, which could be potentially used to disentangle contributions from different atoms in complex compounds. This is a demonstration of the experimental mapping of spin waves in three dimensions by RIXS. It could open the way for other similar measurements, without being confined to 2D materials, and to the investigation of heterostructures, junctions, or patterned samples.

ACKNOWLEDGMENTS

We would like to thank Kurt Kummer, Andrea Amorese, and Karsten Rode for fruitful discussions.

[1] L. J. P. Ament, G. Ghiringhelli, M. Moretti Sala, L. Braicovich, and J. van den Brink, Phys. Rev. Lett. **103**, 117003 (2009).
[2] M. Guarise, B. Dalla Piazza, M. Moretti Sala, G. Ghiringhelli, L. Braicovich, H. Berger, J. N. Hancock, D. van der Marel, T. Schmitt, V. N. Strocov, L. J. P. Ament, J. van den Brink, P.-H. Lin, P. Xu, H. M. Rønnow, and M. Grioni, Phys. Rev. Lett. **105**, 157006 (2010).
[3] L. Braicovich, J. van den Brink, V. Bisogni, M. M. Sala, L. J. P. Ament, N. B. Brookes, G. M. De Luca, M. Salluzzo, T. Schmitt, V. N. Strocov *et al.*, Phys. Rev. Lett. **104**, 077002 (2010).
[4] M. W. Haverkort, Phys. Rev. Lett. **105**, 167404 (2010).
[5] Y. Yamamoto and T. Nagamiya, J. Phys. Soc. Jpn. **32**, 1248 (1972).
[6] W. L. Roth, J. Appl. Phys. **31**, 2000 (1960).
[7] H. Kondoh and T. Takeda, J. Phys. Soc. Jpn. **19**, 2041 (1964).
[8] T. Yamada, J. Phys. Soc. Jpn. **21**, 664 (1966).
[9] T. Yamada, S. Saito, and Y. Shimomura, J. Phys. Soc. Jpn. **21**, 672 (1966).
[10] M. T. Hutchings and E. J. Samuelsen, Phys. Rev. B **6**, 3447 (1972).
[11] A. Picone, M. Riva, A. Brambilla, A. Calloni, G. Bussetti, M. Finazzi, F. Ciccacci, and L. Duò, Surf. Sci. Rep. **71**, 32 (2016).

[12] T. Hibma and M. W. Haverkort, *Magnetic Properties of Antiferromagnetic Oxide Materials* (Wiley-VCH, Weinheim, 2010), pp. 99–142.
[13] S. J. Joshua and A. P. Cracknell, J. Phys. C **2**, 24 (1969).
[14] S. J. Joshua and F. D. Morgan, Phys. Status Solidi B **59**, 269 (1973).
[15] T. Kotani and M. van Schilfgaarde, J. Phys.: Condens. Matter **20**, 295214 (2008).
[16] G. Fischer, M. Däne, A. Ernst, P. Bruno, M. Lüders, Z. Szotek, W. Temmerman, and W. Hergert, Phys. Rev. B **80**, 014408 (2009).
[17] F. Essenberger, S. Sharma, J. K. Dewhurst, C. Bersier, F. Cricchio, L. Nordström, and E. K. U. Gross, Phys. Rev. B **84**, 174425 (2011).
[18] T. Archer, C. D. Pemmaraju, S. Sanvito, C. Franchini, J. He, A. Filippetti, P. Delugas, D. Puggioni, V. Fiorentini, R. Tiwari *et al.*, Phys. Rev. B **84**, 115114 (2011).
[19] Y. O. Kvashnin, O. Grånäs, I. Di Marco, M. I. Katsnelson, A. I. Lichtenstein, and O. Eriksson, Phys. Rev. B **91**, 125133 (2015).
[20] F. M. F. de Groot, P. Kuiper, and G. A. Sawatzky, Phys. Rev. B **57**, 14584 (1998).
[21] G. Ghiringhelli, A. Piazzalunga, C. Dallera, T. Schmitt, V. N. Strocov, J. Schlappa, L. Patthey, X. Wang, H. Berger, and M. Grioni, Phys. Rev. Lett. **102**, 027401 (2009).
[22] M. Tachiki, T. Hosomi, and T. Kobayashi, Jpn. J. Appl. Phys. **39**, 1817 (2000).
[23] K. Marre and H. Neddermeyer, Surf. Sci. **287**, 995 (1993).
[24] N. B. Brookes (unpublished).
[25] L. J. P. Ament, M. Van Veenendaal, T. P. Devereaux, J. P. Hill, and J. Van Den Brink, Rev. Mod. Phys. **83**, 705 (2011).
[26] G. Ghiringhelli, M. Matsubara, C. Dallera, F. Fracassi, R. Gusmeroli, A. Piazzalunga, A. Tagliaferri, N. B. Brookes, A. Kotani, and L. Braicovich, J. Phys.: Condens. Matter **17**, 5397 (2005).
[27] M. W. Haverkort, M. Zwierzycki, and O. K. Andersen, Phys. Rev. B **85**, 165113 (2012).
[28] The parameters used for the simulations are similar to what can be found in Ref. [27]. In detail, we used $10Dq = 0.6$ eV and $\Delta = 5$ eV, while the Slater parameters were reduced to 76.5% of the atomic value.
[29] D. Alders, L. H. Tjeng, F. C. Voogt, T. Hibma, G. A. Sawatzky, C. T. Chen, J. Vogel, M. Sacchi, and S. Iacobucci, Phys. Rev. B **57**, 11623 (1998).
[30] M. W. Haverkort, S. I. Csiszar, Z. Hu, S. Altieri, A. Tanaka, H. H. Hsieh, H.-J. Lin, C. T. Chen, T. Hibma, and L. H. Tjeng, Phys. Rev. B **69**, 020408 (2004).
[31] R. E. Dietz, G. I. Parisot, and A. E. Meixner, Phys. Rev. B **4**, 2302 (1971).
[32] R. Coy, C. Tompson, and E. Gürmen, Solid State Commun. **18**, 845 (1976).
[33] D. C. Tsui, R. E. Dietz, and L. R. Walker, Phys. Rev. Lett. **27**, 1729 (1971).
[34] R. Shanker and R. A. Singh, Phys. Rev. B **7**, 5000 (1973).
[35] K. W. Plumb, A. T. Savici, G. E. Granroth, F. C. Chou, and Y.-J. Kim, Phys. Rev. B **89**, 180410 (2014).